*Earthquake Engineering, Tenth World Conference © 1992 Balkema, Rotterdam. ISBN 90 5410 060 5*

# Topographical site response for harmonic and pseudo-earthquake motions

Hirokazu Takemiya & Tatsuo Tomono
*Department of Civil Engineering, Okayama University, Japan*

**ABSTRACT:** Presented are the site analysis of specific alluvium deposits for harmonic and pseudo-seismic waves incidences, focussing upon the topographical effect on the surface response. Formulation has been conducted using the hybrid method between the finite element for the near field and the boundary element method for the infinitely extending far field. Through the numerical computations, some useful findings are obtained for the wave scattering and propagation due to the subsurface irregularity of alluvium.

## 1. INTRODUCTION

In view of past seismic damages, the 2-dimensional soil amplification with modified predominant period should be pointed out. An extensive frequency response analysis has been conducted primarily to investigate the soil amplification. Another important aspect is the phase characteristic of wave propagation and scattering due to the presence of surface / subsurface soil irregularities. The computation of response time history is essential for this purpose.

Reviewing recent related works, we note the finite difference method (FDM), the finite element method (FEM), the boundary element method (BEM), and the FEM-BEM combination via substructure approach. In utilizing hybrid method special care should be given when formulating the displacement and traction matching between two modelings for which different interpolation functions in space discretization and different time steps may normally be employed.

This paper addresses the 2-dimensional alluvium analysis for wave incidences such as sinusoidal wave, pseudo-earthquake motions which are constructed by a set of Ricker wavelets. Coupling for FEM and BEM domains is taken by use of the weighted residual technique; specifically in the frequency domain analysis over space variable and in the time domain analysis over time steps. The details of the formulation is referred to related authors works.

## 2. FREQUENCY DOMAIN ANALYSIS

### 2.1 BEM (Source force method) for Far Field

We assume that the scattered wave field will be reproduced by imposing a set of appropriately distributed fictitious forces $\mathbf{P}$ on a location $S_b'$ (offset by a small distance from the actual interface $S_b$ of the alluvium boundary for the computational reasons) in the free field. This intermediate quantity is determined by the weighted residual technique for the actual displacement $\mathbf{u}^s$ and traction $\mathbf{t}^s$, and the pseudo-counterparts $\mathbf{u}^s_p$ and $\mathbf{t}^s_p$ due to $\mathbf{P}$.

$$\int_{S_b} \mathbf{w}_d^T(y)(\mathbf{u}^s(y) - \mathbf{u}^s_p(y))\, ds(y) = 0 \tag{1}$$

$$\int_{S_b} \mathbf{w}_t^T(y)(\mathbf{t}^s(y) - \mathbf{t}^s_p(y))\, ds(y) = 0 \tag{2}$$

The relevant Green functions for displacement $\mathbf{G_u(y,x)}$ and traction $\mathbf{G_t(y,x)}$ for point / uniformly distributed forces are needed for the response computation. (Takemiya and Arioka, 1991) Taking the weighting functions as $\mathbf{w_d(y)= G_t(x,y)}$ and $\mathbf{w_t(y)= G_u(x,y)}$ leads

$$\int_{S_b}\int_{S_b} \mathbf{G_t}(x,y)\mathbf{u}^s(y)ds(y) = \int_{S_b}\int_{S_b} \mathbf{G_u}(x,y)\mathbf{G_t}(y,x')\mathbf{p}(x')ds(x')ds(y) \tag{3}$$

The discretized form for Eq.(3) results in

$$\mathbf{H}\,\hat{\mathbf{u}}^s_{b,BEM} = \mathbf{G}^T\mathbf{P} \tag{4}$$

Then, the total wave representation becomes

$$\mathbf{H}\,(\hat{\mathbf{u}}_{b,BEM} - \hat{\mathbf{u}}^f_b) = \mathbf{G}^T\mathbf{P} \tag{5}$$

in which $\hat{\mathbf{u}}^f_b$ is the discretized value of free field response by the assumed incident wave.

### 2.2 FEM for Near Field

Following the familiar procedure, the discretized FEM governing equation is expressed as

$$\begin{bmatrix} \mathbf{D}_{ii} & \mathbf{D}_{ib} \\ \mathbf{D}_{bi} & \mathbf{D}_{bb} \end{bmatrix}_{BEM} \begin{Bmatrix} \hat{\mathbf{u}}^n_i \\ \hat{\mathbf{u}}^n_b \end{Bmatrix}_{BEM} = \begin{Bmatrix} 0 \\ \int_{S_b} \mathbf{N}^T \mathbf{t}^n_b ds \end{Bmatrix}_{BEM} \tag{6}$$

in which $\mathbf{D}$'s define the dynamic stiffness matrices

$$\mathbf{D}^n = -\,\omega^2 \mathbf{M}^n + i\,\omega \mathbf{C}^n + \mathbf{K}^n \tag{7}$$

with $\mathbf{M}$, $\mathbf{C}$ and $\mathbf{K}$ denoting, respectively the mass, damping and stiffness matrices, the subscript "i" indicates the internal nodes and "b" the boundary nodes, and $i$ = imaginary unit.

### 2.3 Hybrid Procedure

The governing equation of the coupled system for the above BEM and FEM domains is made such that the degrees of freedom (DOFs) of the FEM are maintained and the far field impedance function derived from the BEM analysis, which is compatible with the DOFs of the interface boundary, is substituted into the former equation. The weighted residual equations for displacement and traction are used for this purpose.

$$\int_s w_d^T(y)(u_{b,BEM} - u_{b,FEM})\, ds(y) = 0 \quad (8)$$

$$\int_s w_t^T(y)(t_{b,BEM} + t_{b,FEM})\, ds(y) = 0 \quad (9)$$

in which the weighting functions $w_d(y)$ and $w_t(y)$ are adopted as follows:

$$w_d(y) = t_p^s(y) \quad \text{and} \quad w_t(y) = u_b(y) \quad (10),(11)$$

After discretization, Eqs.(8) and (9) result in

$$G^T P + H(u_b^f - \hat{u}_{b,BEM}) = 0, \quad H^T P + P_b^f + P_{b,BEM} = 0 \quad (12),(13)$$

The far field impedance $K_{bb}^*$ and the effective input force $P_b^f$ to the FEM domain are derived by eliminating the unknown force intensities $P$ from Eqs.(12) and (13). Hence, the total governing equation results.

$$\begin{bmatrix} D_{ii}^n & D_{ib}^n \\ D_{bi}^n & D_{bb}^n + K_{bb}^* \end{bmatrix} \begin{Bmatrix} \hat{u}_i^n \\ \hat{u}_b^n \end{Bmatrix} = \begin{Bmatrix} \hat{P}_i^n \\ K_{bb}^* \hat{u}_b^f - \hat{P}_b^f \end{Bmatrix} \quad (14)$$

with $\quad K_{bb}^* = H^T (G^T)^{-1} H$

## 3. TIME DOMAIN FORMULATION

### 3.1 Incident Waves

Velocity-type Ricker wavelets have been used as simple but meaningful incident waves at the far field.

$$\dot{u}^I(x,z,t) = a\, V(\alpha^I)\, H(\alpha^I) \quad (15)$$

in which $V(\alpha^I)$ denotes a function to describe the wave form.

$$V(\alpha^I) = \left[ 2\left(\frac{\pi}{\lambda_s}\alpha^I\right)^2 - 1 \right] \exp\left\{ -\left(\frac{\pi}{\lambda_s}\alpha^I\right)^2 \right\} \quad (16)$$

The representative wave length $\lambda_s = V_s T_p$ is assumed in which $V_s$ denotes the shear velocity and $T_p$ gives the representative period. The function $H(\,)$ stands for the Heaviside step function and $a$ is the intensity. The argument $\alpha^I$ indicates the phase to be specified at a location $(x_0, z_0)$ at initial time $t_0$ as

$$\alpha^I = V_s(t-t_0) - \sin\theta(x-x_0) + \cos\theta(z-z_0) \quad (17)$$

The associated displacement and acceleration are obtained by the integration and differentiation respectively of Eq.(15). Hence,

$$D(\alpha^I) = 2\frac{\pi}{\lambda_s}\alpha^I \exp\left\{ -\left(\frac{\pi}{\lambda_s}\alpha^I\right)^2 \right\} \quad (18)$$

$$A(\alpha^I) = \frac{\pi}{2\lambda_s}\alpha^I \left\{ 3 - 2\left(\frac{\pi}{\lambda_s}\alpha^I\right)^2 \right\} \exp\left\{ -\left(\frac{\pi}{\lambda_s}\alpha^I\right)^2 \right\} \quad (19)$$

The counterparts in the frequency domain are given respectively as

$$i\omega D(\omega, T_p, t_0) = V(\omega, T_p, t_0) = \frac{A(\omega, T_p, t_0)}{i\omega} \quad (20)$$

$$V(\omega, T_p, t_0) = -\frac{\pi T_p \omega^2}{4} \exp\left[ -\frac{T_p^2}{4\pi^2} - i\omega t_0 \right] \quad (21)$$

Pseudo-earthquake motions are simulated by superimposing a set of Ricker wavelets of different representative periods and arriving times.

$$\dot{u}^I(x,z,t) = \sum_{k=1}^{N} a_k \dot{u}_k^I(x,z,t-t_0^k) \quad (22)$$

### 3.2 FEM for Near Field

The alluvium soil deposits which may have irregular distribution of soil properties are modeled by the quadratic finite elements. The standard procedure yields the governing equation of the mass, damping and stiffness matrix $M$, $C$, and $K$ for any time step $K$, as

$$M\ddot{U}^K + C\dot{U}^K + KU^K = F_F^K(t) \quad (23)$$

with certain traction $F(t)$ acting along the boundary due to the effect of the extending soil medium. The viscous damping effect is taken into account which gives rise to a damping ratio h for the fundamental mode when the alluvium is fixed along the boundary.

### 3.3 BEM for Far Field

The time domain boundary element method is applied with use of the geometric linear interpolation function and stepwise time variation. The double analytical integrals over elements for the product of the fundamental solution and the interpolation function are performed by the Cagniard-de Hoop method [Wang and Takemiya, 1992]. Hence, we get a time stepping algorithm for the scattering wave field.

$$H^0 U^K - G^0 T^K = -\sum_{k=1}^{K} \left( H^k U^{K-k} - G^k T^{K-k} \right) = -F^K \quad (24)$$

in which $U^K$ and $T^K$ are the displacements and tractions associated with nodes on the interface as well as along the free surface, and the matrices $H$ and $G$ are determined based on the linear and constant element assumption respectively. The total wave representation of incident and scattering waves for Eq.(24) becomes

$$H^0(U^K - U^{IK}) - G^0(T^K - T^{IK}) = -F^K \quad (25)$$

in which $U^{IK}$ and $T^{IK}$ denote respectively the discretized displacement and traction values at nodes for a specified incident wave. For the wave field analysis of an alluvium on a uniform / layered halfplane, the substructure procedure is effectively used [Takemiya, Wang and Fujiwara, 1991]. After differentiating nodes at free surface from those on the interface and then condensing out other variables than those related to their interface, the governing equations for the exterior domain are expressed with the interface variables as unknown quantities. Expression for the force-displacement relationship by defining the dynamic stiffness matrix becomes

$$F_B^K(t) = K_B U^K - F_{F..}^{0,K}(t) \quad (26)$$

in which $F^0$ defines the input force to the alluvium.

3.4 Hybrid Procedure

In the BEM the traction variation in time is assumed as a piecewise constant whose time increment $\Delta t_B$ is normally longer than that of the FEM, since the former takes account of the inertial effect already in the Green function while the latter evaluates it after the discretization. The equilibrium and compatibility conditions are now considered at the FEM time increment, $\Delta t_F$. The FEM for dynamic problems demands an interpolation functions of at least the 2nd order to connect the neighboring 3 nodes for the displacement variation and the corresponding derivative concerns the traction distribution. The BEM, on the other hand, thereby assumes the 1st order interpolation function between adjacent nodes for the same response quantity and the 0-th order for the traction. The matching is taken by use of the weighted residual method because of the differences in the assumption of traction variation in time.

$$\int_{-1}^{+1} W(\xi)\{F_B(\xi) - F_F(\xi)\}d\xi=0 \qquad (27)$$

in which $W(\xi)$ is the weighting function with the isoparametric local variable $\xi$. The representation of the current displacement, velocity and acceleration in terms of the previous corresponding nodal values is made. The due consideration of the acceleration effect demands taking the 2nd order interpolation. Substituting Eqs.(23) and (26) into Eq.(27) leads [Takemiya and Tomono, 1992].

$$\left[M_F +\gamma\Delta t_F C_F+\beta(\Delta t_F)^2 K_F+\alpha(\Delta t_F)^2 K_B\right] U^{K+i/N} +$$
$$\left[-2M_F +(1-2\gamma)\Delta t_F C_F+(1/2-2\beta+\gamma)(\Delta t_F)^2 K_F+(1-\alpha)(\Delta t_F)^2 K_B\right]$$
$$\times$$
$$U^{K+(i-1)/N}$$
$$+\left[M_F -(1-\gamma)\Delta t_F C_F+(1/2+\beta-\gamma)(\Delta t_f)^2 K_F\right] U^{K+(i-2)/N}$$
$$= \alpha(\Delta t_F)^2 K_B^{0,K+i/N}+(1-\alpha)(\Delta t_F)^2 K_B^{0,K+(i-1)/N};\ 0\le i\le N \qquad (28)$$

in which the weighting function is chosen as $w(\xi)=|\xi|$ so that $\alpha=1/2$, $\beta=1/4$ and $\gamma=1/2$.

## 4. NUMERICAL COMPUTATION AND FINDINGS

For the present numerical computation, the trapezoidal-shape alluvium, as shown in Fig.1, is considered. The soil properties are indicated in Table 1. A typical soil impedance ratio is chosen between the near and far field. The finite element meshes are used for the modeling of the soft soil deposits together with some portion of the neighboring far field to make the computation stable.

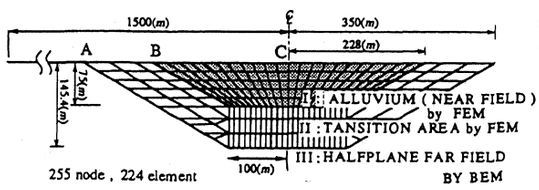


Fig.1 Model for analysis

For the steady state harmonic analysis (Takemiya, Ono, and Suda, 1991), the parametric study has been conducted with regrards to the type of the incident wave such as SH-, P-, SV-, Rayleigh waves and the angle of the incidence at some representative non-dimensional frequencies as defined by the ratio of the surface width of alluvium 2A to the incident wave length $\lambda$, i.e. $\eta = 2A/\lambda$. Some illustrative results for the SH and SV wave incidences of vertical direction are shown in Fig.2 and 3. Besides the indirect BEM solution for the far field, the direct BEM solution is also included for the purpose of verifying its accuracy. Special attention shold be paid to the soil layering, noting the difference between the 2-dimensional and the 1-dimensional wave propagations in the frequency range, which is crucial in the seismic viewpoint. Remarks on other wave and oblique incidences are referred to in the above work. The variation in surface amplifications are closely related to the topography and the dimensionless frequency. Such response characteristics give a good interpretation of the actual seismic waves amplification and the generation of surface waves.

The transient time domain analysis, in contrast to the frequency domain analysis, makes clear the response features of the topographical site condition with respect to the phase in wave propagation. Since the detail response investigation for a single Ricker wavelet incidence has been made elsewhere [Takemiya, Wang and Fujiwara, 1991; Takemiya and Tomono, 1992], the results for representative pseudo-earthquake input motions which are constructed based on a set of Ricker wavelets superimpositions are shown. Two distinct motions are generated as depicted in Figs. 4 and 5.; short period and long period waves, which are composed of the same relative frequency contents but different amplitudes for each consecutive 1 second duration. Their total frequency spectral densities are depicted in the same figures. Figs. 6. and 7 show the resulting surface responses in time histories for displacement and acceleration components. Because of the symmetry only half surface locations are chosen for indication. One can see the wave propagation clearly in the displacement and acceleration time histories. The response for the short period incident wave results in a more complex wave scattering and propagation than that for the long period incidence. Their maximum value profiles are given in Figs. 8 and 9. It should be noted that for the present soil impedance ratio the motion of the soft soil deposits are dominating the response. Threfore, when the short period incident wave is used, it indicates the amplification for displacement component while deamplification for acceleration component. When the long period incident wave is used, the amplification is observed both at the displacement and acceleration responses. The The same trend is observed in the companion paper by FEM with soil nonlinearity considered. [Takemiya and Ishiyama 1992].

Table 1 Soil Properties

| | Shear velocity | Density | Damping ratio | Poisson ratio |
|---|---|---|---|---|
| Alluvium Deposit | 200 m/s | 1.6 t/m³ | 0.10 | 0.45 |
| Far Field | 500 m/s | 2.0 t/m³ | 0.02 | 0.35 |

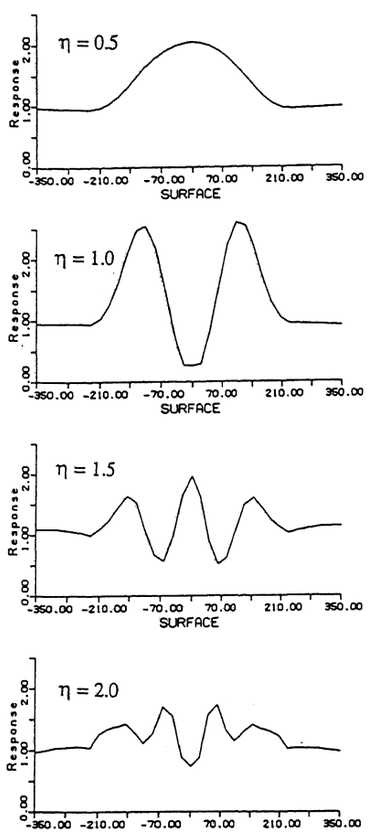


Fig.2. Surface amplification,
Vertical harmonic SH wave incidence

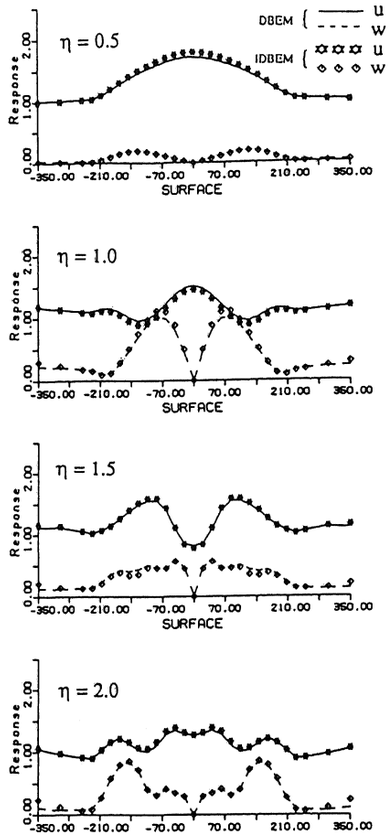


Fig.3 Surface amplification,
Vertical harmonic SV wave incidence

The comparison with the 1-dimensional solution for the same incident wave makes clear the 2-dimensional effect. In Figs. 6 and 7 the corresponding time histories for displacement and acceleration are shown together for easy comparison. A little difference is observed for the long-period incident wave from the 2-dimensional wave propagation; however, significant differences are observed for the short-peirod incident wave. Almost the same maximum response values are predicted for displacement, but not for acceleration.

## 5. CONCLUSION

The advantage of the hybrid method utilizing BEM and FEM is demonstrated for the seismic analysis of topographical alluvium deposits underlaid by a halfplane medium. From the numerical computation, such site effects, which are indicated as the difference from the far field response and also from the 1-dimensional soil column analysis of the concerned soil deposits, is clarified with respect to the amplification as well as to the phase in wave propagation. The results observed from psuedo-earthquake motions of short period indicate the displacement amplification and the acceleration deamplification. However, the long period motion showed both the displacement amplification and acceleration amplification.

## REFERENCES

Takemiya, H. and Arioka, K.(1991), Numerical Evaluation of Green's Function of Layered Viscoelastic Halfplane for Certain Buried Forces, 7th Int. Conf. Comp. Meth. Advances in Geomech., Cairns, 1091-1096.

Takemiya, H. and Ono, M. and Suda, K.(1991), BEM-FEM Hybrid Analysis for Topographical Site Response Characteristics, Proc. Int. Conf. Geotech. Earthq. Eng. Soil Dyn. ASCE,Missouri-Rolla. AS CE.

Wang, C.Y. and Takemiya, H.(1992), Analytical Elements of Time Domain BEM for Two-Dimensional Scalar Wave Problems, Int. J. Num. Meth. Eng., Vol.32,No.2

Takemiya, H., Wang, C.A. and Fujiwara, A.(1991), Transient Response of Certain Topographical Sites for SH-wave Incidence, 5th Soil Dyn. Earthq. Eng., Karlsruhe, 139-150.

Takemiya, H. and Tomono,T.(1992), Transient Topo-graphical Site Response Analysis by Time Domain Hybrid Method, Proc. EGS1992. Odawara. Japan.

Takemiya, H. and Ishiyama, M.(1992), Nonlinear 2-Dimensional Seismic Response of Soil Deposits, Proc. EGS1992. Odawara. Japan.

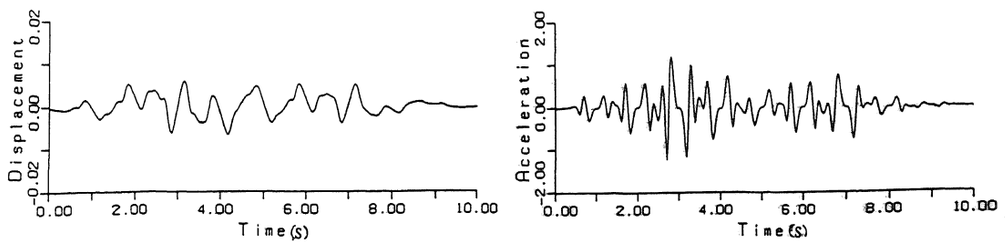


(a) Time history

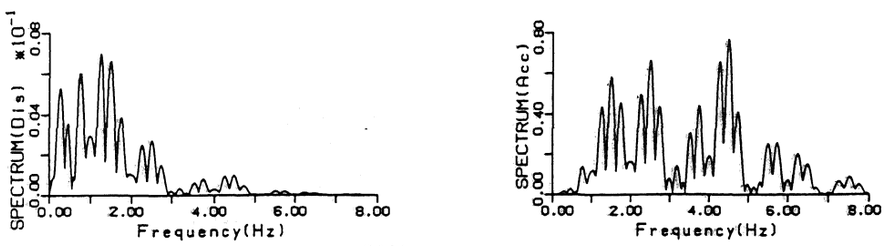


(b) Frequency contents

Fig.4 Pseudo-earthquake motion, Short period type

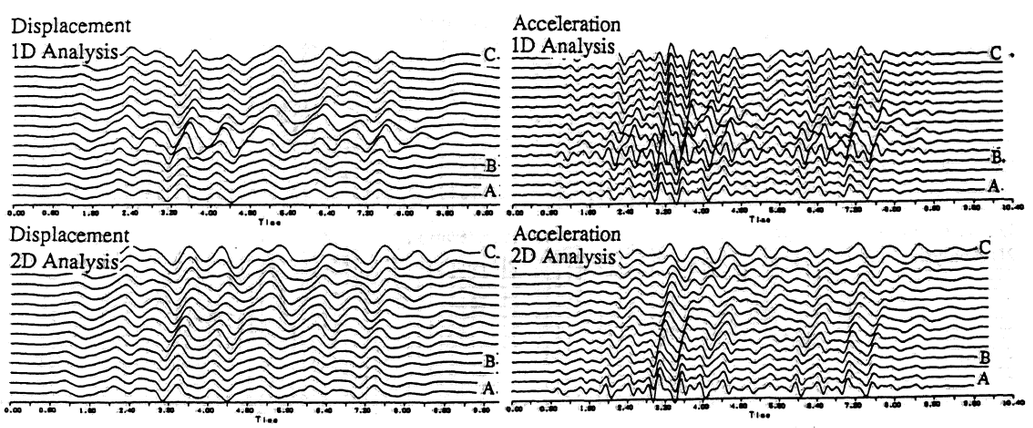


Fig.6 Surface response due to short-period type pseudo-earthquake motion

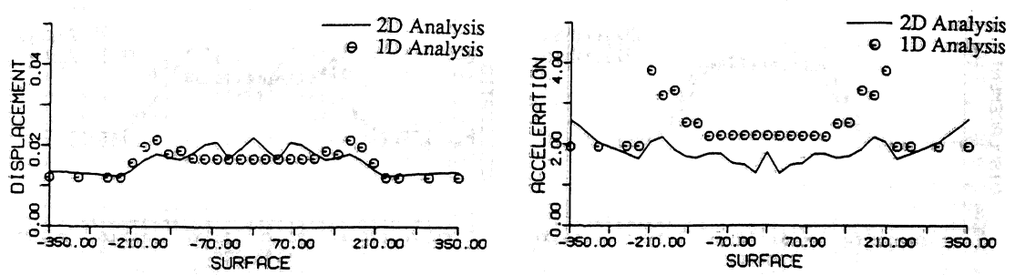


Fig.8 Maximum surface response profile
for short-period type pseudo-earthquake motion

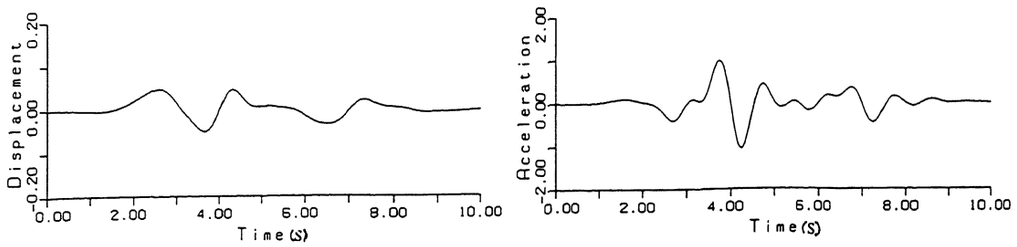


(a) Time history

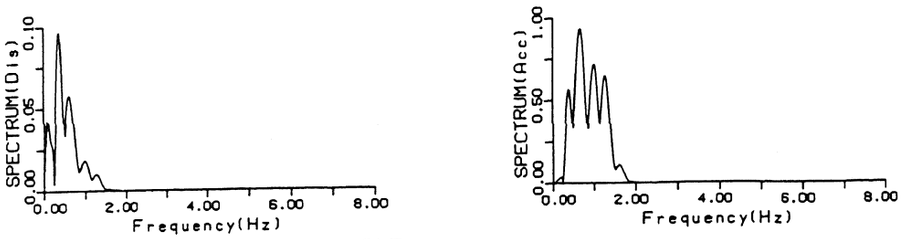


(b) Frequency contents

Fig.5 Pseudo-earthquake motion, Long-period type

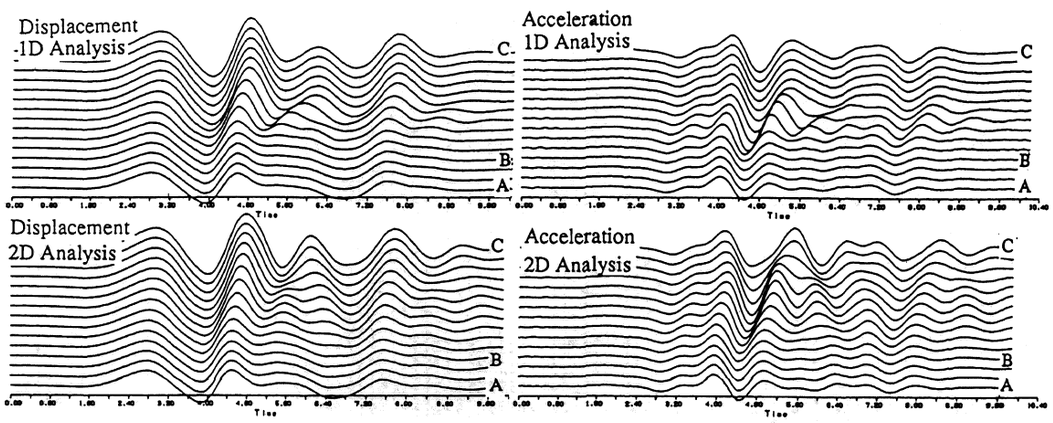


Fig.7 Surface response due to long-period type pseudo-earthquake motion

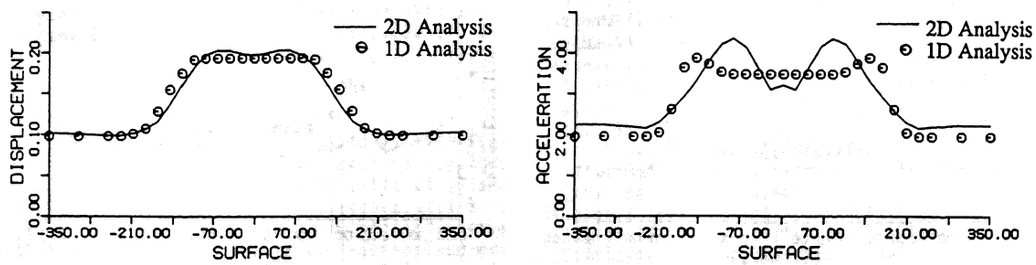


Fig.9 Maximum surface response profile
for long-period type pseudo-earthquake motion